Structural and Temperature-dependent vibrational analyses of the non-centrosymmetric ZnMoO$_4$ molybdate

H. Ait ahsaine[a,b]*, M. Zbair[c], M. Ezahri[a], A. Benlhachemi[a],
B. Bakiz[a], F. Guinneton[b], J-R. Gavarri[b]

[a] Laboratoire Matériaux et Environnement LME, Faculté des Sciences, Université Ibn Zohr, BP 8106, Cité Dakhla, Agadir, Maroc

[b] Institut Matériaux Microélectronique et Nanosciences de Provence, IM2NP, UMR CNRS 6242, Université de Toulon, BP 20132, 83957, La Garde Cedex, France

[c] Laboratoire de catalyse et corrosion des matériaux, Université Chouaib Doukkali, Faculté des sciences El Jadida, BP. 20, El Jadida 24000, Maroc

Abstract

The triclinic phase of zinc molybdate ZnMoO$_4$ was synthesized by a simple co-precipitation method followed by calcination at different temperatures. Thermal differential and thermogravimetry analyses were performed under air. The polycrystalline samples of ZnMoO$_4$ compound obtained with different thermal treatments were characterized by X-ray diffraction, cell parameters were determined using Lebail fit analyses and the crystallites size was calculated using Scherrer equation. Fourier transform infrared and Raman spectroscopy analyses were investigated and discussed, all the bands were assigned the corresponding vibrations. Correlation with structural and thermal analyses was made.

Keywords: Zinc molybdate, Co-precipitation method, Vibrational analyses, crystallite size.

1. Introduction

Tungstates and molybdates of MWO$_4$ or MMoO$_4$ type have multiple properties with interesting applications in the fields of catalysis, photocatalysis and luminescence. The formation mechanisms and the stability of their solid solutions were recently analyzed [1-2]. For instance, *Tomszewicz et al* report the synthesis and the study of the new rare-earth metal molybdates and tungstates [3-4] while G.H. Lee reports the rare earth (Eu) doped metal tungstates as a red phosphor for white LEDs [5]. In a recent study, we developed a new bismuth lutetium tungstate compound belonging to the same family of the High-temperature Bismuth tungstate [6].

In the last decades, zinc molybdate ZnMoO$_4$ was extensively studied for its high potential in industrial applications. This molybdate was investigated for its luminescence properties [7-10], for applications in bolometers, scintillation detectors [11-15], humidity sensors [16], photocatalysis [17-19], microwave dielectric devices [20] and battery electrodes [21]. Traditionally, two phases α- and β-Zinc molybdate have been synthesized by different techniques, such as hydrothermal method [22-24], solid state reaction [25-30], citrate

complex precursors [31], co-precipitation method [32-35], electrospinning calcination method [36] and electrochemistry assisted ablation laser method [37]. Gaoke and co-workers have reported a phase transition from α- $ZnMoO_4$ (triclinic, space group P -1) to β- $ZnMoO_4$ (Monoclinic, space group P2/c) at about 462°C by the mean of DSC analyses and curves [38].

Recently [39], we have observed the phase transition in the $ZnMoO_4$ ceramics through the study of electrical properties. The bulk conductivity is characterized by a complex modification occurring above the transition point (presently Tc = 723 K or Θ_c = 450°C). Using a model based on two behaviors of charge carriers, coupled with the phase transition mechanism, we have simulated the conductivity as temperature increases. In this present study, we report the effect of calcination temperature on the structural properties of ZMO powders, DTA-TGA analyses of the $ZnMoO_4$ precursor were fully discussed. A first study to discuss the effect of temperature on Raman vibrational properties of $ZnMoO_4$ and the influence of defects and elaboration conditions on its properties.

2. Experimental

2.1 Synthesis of ZMO samples

Zinc molybdate was synthesized via a co-precipitation method using sodium molybdate ($Na_2MoO_4.2H_2O$) and zinc nitrate ($Zn(NO_3)_3.6H_2O$) [35]. A mixed aqueous solution was prepared by dissolving required weights of appropriate amounts of $Zn(NO_3)_3.6H_2O$ and Sodium molybdate $Na_2MoO_4.2H_2O$ in 50ml of distilled water in separated beakers with magnetic stirring. Then sodium molybdate solution was gradually added to the zinc nitrate solution. The resulting white precipitate was filtered and washed several times with distilled water and ethanol, and finally thermally treated at various temperatures of 300°C, 400°C, 500°C and 600°C, during 3 hours (samples noted $ZnMoO_4$-Θ with Θ = 300, 400, 500, 600).

2.3 *Characterization of ZMO ceramics*

The X-Ray diffraction patterns were collected using an EMPYREAN PANALYTICAL diffractometer operating at 45 kV/35 mA, using CuKα radiation with Ni filter, and working in continuous mode with a step size of 0,013°. Data were collected over a range 5-80° 2θ. Differential thermal analyses coupled with thermogravimetry were performed to determine the dehydration kinetics of prepared samples. The thermal decomposition of the precursor was followed under air from ambient temperature to 1050°C with a rate of 10 °C/min (using Shimadzu Instruments DTG-60 equipment). Fourier Transform Infrared spectrum of $ZnMoO_4$ samples was obtained in the mid infrared region (400-4000cm-1) using a Shimadzu 4800S. The spectra were scanned at resolution of 2.0 cm-1 and with 20 scanning. Raman spectra were recorded on a VERTEX 70 Raman spectrometer using a power of 30 mW and the wavelength of Ar green laser λ=514.5 nm. The frequency bands ν ranged from 50 to 1100 cm^{-1}.

3. Results and discussion

3.1. *X-Ray diffraction analyses*

Figure 1 below, presents the X-ray diffraction patterns of the samples thermally treated at various temperatures Θ=300, 400, 500 and 600°C. All detectable peaks were indexed in conformity with the triclinic space group *P-1* (data from JCPDS 70-5387). The calculated lattice parameters were obtained using Lebail fit and are reported in Table 1. The cell volume is quasi constant. For $ZnMoO_4$-600 sample at 600°C: a = 8.367 Å, b = 9.691 Å and c = 6.964 Å, α=96.70°, β=106.90° and γ=101.70. The four samples present a significant decrease of the full width at half medium of Bragg peaks, as the elaboration temperature Θ increases, reflecting a progressive improving crystallization. **Table 1** gives the values of correlation lengths or crystallite sizes calculated from Scherrer approach. The Williamson-Hall test allowing separating the size effect from the cell distortion gave no significant additional information
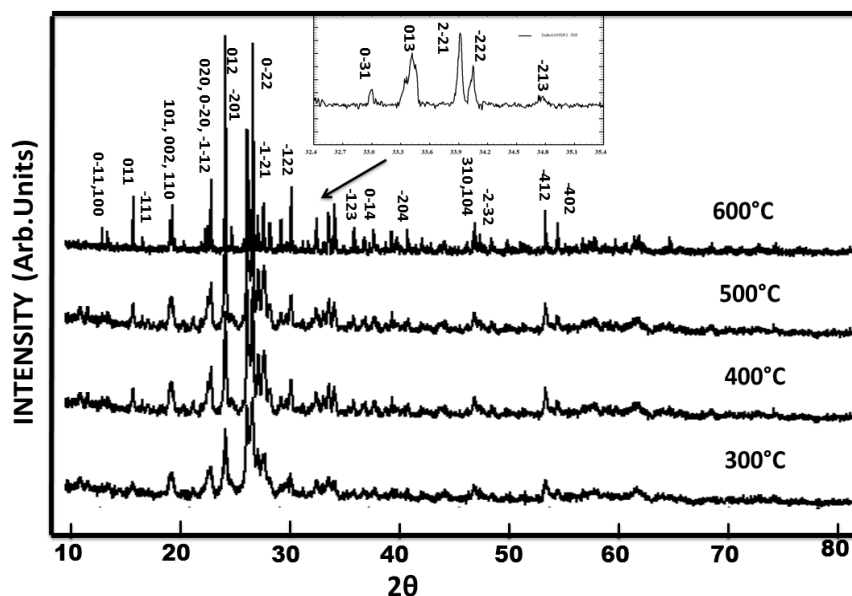
Figure 1: X-Ray diffraction patterns of α-ZnMoO₄ obtained in room conditions, after thermal treatments at 300°C, 400°C, 500°C and 600°C, during 3 hours.

The Scherrer equation relates the full width at half maximum of Bragg peaks to the average crystallite dimensions or correlation lengths D, characteristic of the grain populations: $D_{hkl} = k.\lambda / (\Delta 2\theta.\cos(\theta))$. In this expression, $\lambda = 1.54056$ Å is the wavelength of the radiations (CuK$_\alpha$ radiation), k = 0.9 for Gaussian profiles, $\Delta 2\theta_{size}$ is the broadening of a Bragg peak due to size effect, depending of Miller indices (hkl) and calculated using the formula: $\beta^2 = (\Delta 2\theta_{size})^2 = (\Delta 2\theta_{exp.})^2 - (\Delta 2\theta_{standard})^2$. The $\Delta 2\theta_{exp.}$ is the observed full width at half maximum of a Bragg peak, the $\Delta 2\theta_{standard}$ is the full width determined from the ZMO-600 sample considered as a standard. Table 1 below reports the lattice parameters and the D values. Recently, we have performed The Rietveld refinements on the ZnMoO₄ ceramics [39].

Table 1: Lattice parameters and crystallite sizes (nm) of the ZnMoO₄-Θ samples

| Triclinic space group P-1, 6 units / cell				
ZMO-Θ	300	400	500	600
a (Å)	6.963(2)	6.961(4)	6.955(4)	6.964(1)
b (Å)	8.362(3)	8.362(2)	8.368(3)	8.369(1)
c (Å)	9.709(2)	9.708(5)	9.707(3)	9.694(2)
α (°)	96.762(2)	96.762(2)	96.759(2)	96.756(2)
β (°)	106.903(2)	106.901(2)	106.897(2)	106.881(2)
γ (°)	101.657(2)	101.657(2)	101.635(2)	101.752(2)
Volume (Å³)	520.13(3)	520.07(4)	520.04(3)	519.79(5)
D (*) Crystallite size (nm)	28 ± 5	56 ± 8	66 ± 9	Standard sample

(*) D is the crystallite size calculated by Scherrer approach

3.2. *Thermal analyses*

Figure 2 shows the Thermal differential and thermogravimetric curves obtained from the white precipitate. From the recorded thermograph of the precursor, it has been observed that the total weight loss is about 9%, we have also observed several endothermic peaks:

- $\Theta < 150°C$: weight loss due to surface water ;
- $150°C < \Theta < 250°C$: weight loss due to lattice water and/or residues;
- $250°C < \Theta < 350°C$: weight loss mainly due to hydroxide decompositions and partly due to residues such as evaporation of various gases such as NO_2, CO_2 and NH_3.
- $\Theta = 520°C$: α➔β phase transition [39].

In the heating process, we observe a shifted transition temperature due to fast heating rate ($\Theta c = 530 \pm 20$ °C): the Thermal differential endothermic signal appears as being spread over a wide temperature range. In the slow cooling process , we observe exothermic peaks due to the crystallization of the β phase (768°C) and to the transition β➔α located at $\Theta_c = 466 \pm 5$ °C in this case. This last temperature is in good agreement with the expected transition temperature, mainly because of the very slow cooling undergone by the sample.
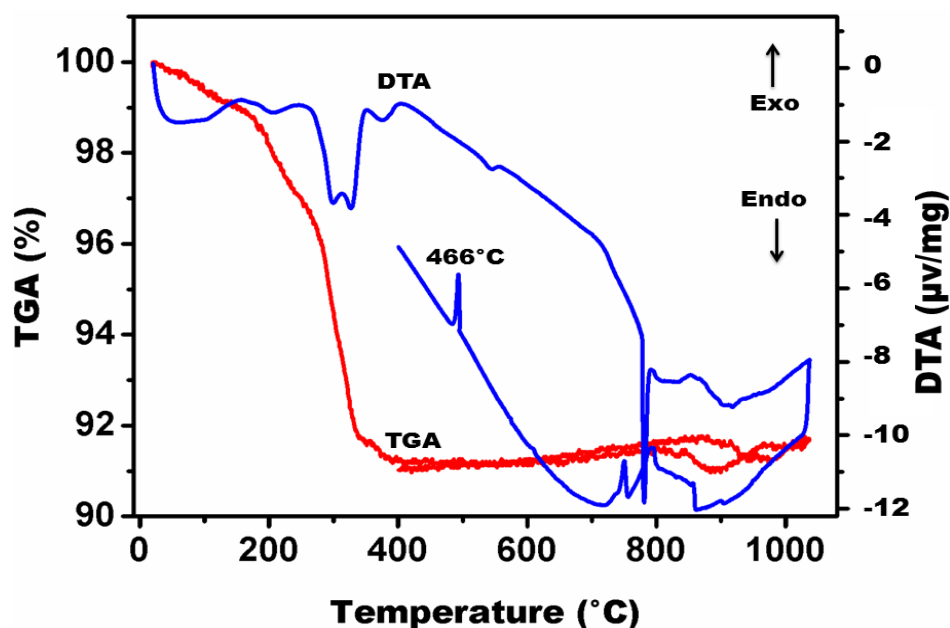

Figure 2: thermographs of the precursor (white gel)

### 3.3. *Infrared and Raman spectroscopy*

To analyze the influence of thermal treatment, the four samples ZMO-600 were characterized by FTIR and Raman spectroscopy. **Figure 3** shows the infrared absorption bands. The vibration modes associated with the frequencies ranging between 750 and 980 cm^{-1} can be attributed to distorted $(MoO_4)^{2-}$ tetrahedrons [40-42]. The attribution of modes has been reported in Table 2. The bands at 1633 and 3435 cm^{-1} correspond to H–O–H bending and O–H stretching vibrations respectively [43,44].

In **Figure 4**, we have reported the Raman spectra of the sample $ZnMoO_4$ samples as a function of temperature. The main Raman peaks of the crystallized sample well crystallized $ZnMoO_4$-600 are located at 340, 370, 400, 790, 812, 850, 889, 918, 940 and 965 cm^{-1}, in agreement with previous works [42,45,46]. The profile analysis of the Raman spectra at high frequencies (790 to 965 cm^{-1}, **Figure 5**) was performed with Magic Plot Pro software and using Lorentzian profiles.

J. Mater. Environ. Sci. 7 (9) (2016) 3076-3083
ISSN : 2028-2508
CODEN: JMESC

Ait ahsaine et al.
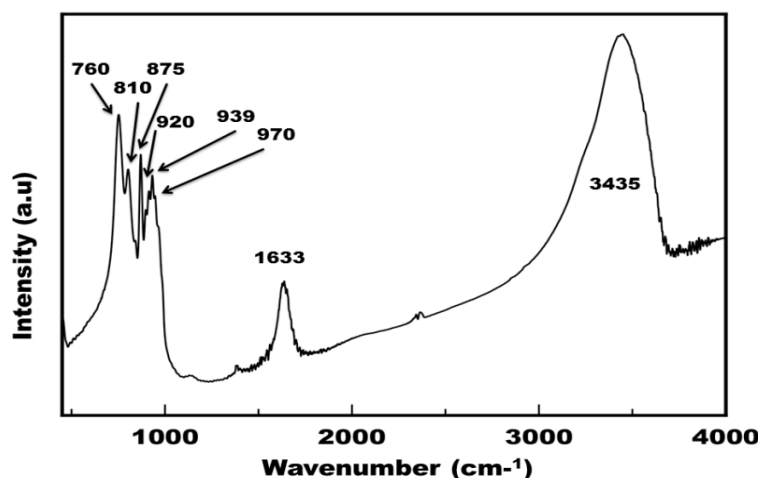
Figure 3: Fourier transformed infrared spectra of the $ZnMoO_4$-600 compound

The change in the Raman intensity can be explained by the fact that the population of any vibrational state is temperature dependent: The population of the ground state is reduced with increasing temperature. Thus stokes bands show reduced intensity. With the excited state it is other way round and thus anti-stokes bands increase with increasing temperature. With regard to the appearing bands, it is well known that temperature affects the crystallinity, therefore the materials (300°C, 400°C, 500°C and 600°C) present different Raman signature, this results are consistent with the XRD analyses which show a lower crystallinity degree for the sample at 300°C. The significant broadening of the vibration bands observed in the case of the ZnMoO4 samples can be directly linked to the presence of structural disorder [47]. Furthermore, the difference in the Raman bands between the $ZnMoO_4$-300°C and the other sample could be due to the presence of precursor impurities that are not decomposed, this has been confirmed by thermal analyses.
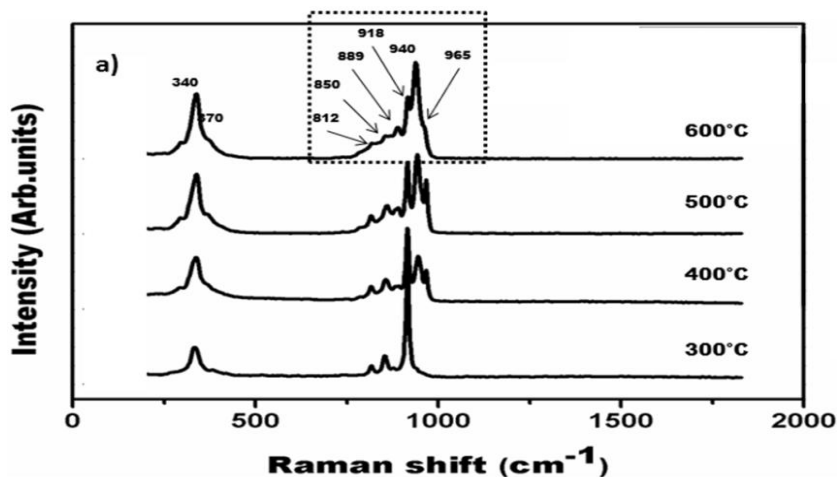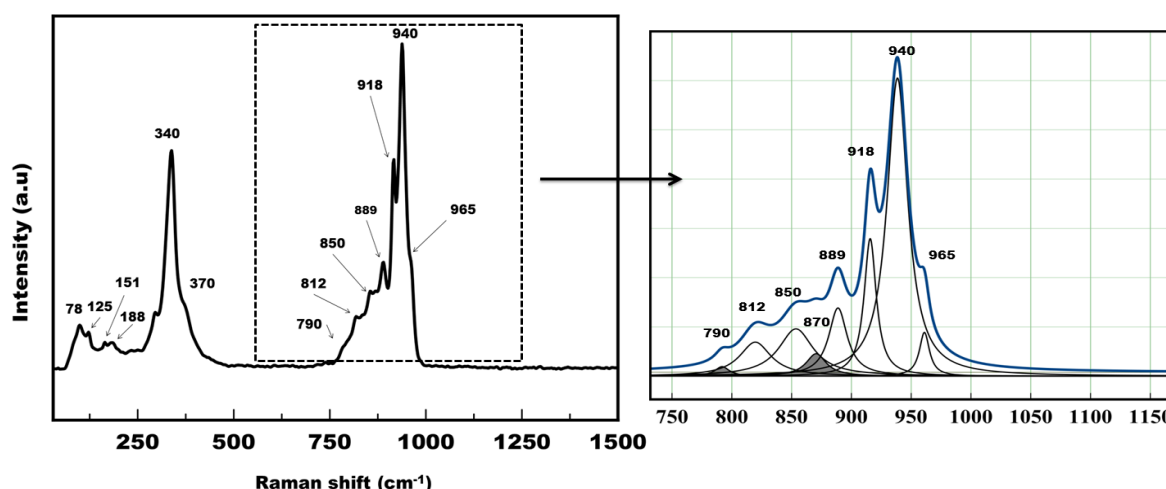

Figure 4: Raman spectra of the $ZnMoO_4$ samples at different temperatures.

As reported by Phuruangrat and co-workers [48] the Raman vibration modes are divided into two features:
  - Internal modes: generated from the oscillation inside the molecular ionic groups with immobile mass center.
  - External modes: it is the lattice phonon vibrations due to the motion of cation M^{2+} metal ions relative the rigid molecular ionic units.

Considering the Td symmetry, four internal modes of MoO_4 free tetrahedrons can be expected and were designated by authors [49,50] as : ν_1 (A_1), ν_2(E), ν_3(F_2), ν_4(F_2). In the case of scheelite structures (tetragonal symmetry, oxygen in tetrahedral configuration), the group theory shows that the crystals have 26 distinct vibration modes (Raman and infrared), with the following representation: $\Gamma_{(Raman + Infrared)} = 3A_g + 5A_u + 5B_g + 3B_u + 5E_g + 5E_u$. Thirteen of these vibration modes noted as $3A_g + 5B_g + 5E_g$ belong to the Raman active modes. It should be recalled that in the case of centrosymmetric molecules the IR and Raman bands have different frequencies. In the case of non-centrosymmetric molecules the exclusion rule vanishes. In the present study the frequencies associated with MoO_4 tetrahedral vibration modes are practically the same in fourier transform infrared and Raman experiments, for sample $ZnMoO_4$-600. This means that MoO_4 molecules should be non-centrosymmetric. Taking into account the very low symmetry of the triclinic structure, we can expect a complex splitting of these fundamental vibrations. Table 2 summarizes all the vibration modes of the as-prepared $ZnMoO_4$-600 sample.

Figure 5: Decomposition of the A_1 stretching mode at high shifts.

Table 2: Vibration modes from Raman spectroscopy data of the $ZnMoO_4$-600 sample

Mode	Raman frequencies in cm^{-1}	FTIR frequencies in cm^{-1}	Attribution
ν_1 (A_1)	965	970	MoO_4: symmetric stretching
ν_1 (A_1)	940	939	MoO_4: symmetric stretching
ν_1 (A_1)	918	920	MoO_4: symmetric stretching
ν_1 (A_1)	889	__	MoO_4: symmetric stretching
ν_3(F_2)	870	875	MoO_4 : antisymmetric stretching
ν_3(F_2)	850	__	MoO_4 : antisymmetric stretching
ν_3(F_2)	812	810	MoO_4 : antisymmetric stretching
ν_3(F_2)	790	760	MoO_4 : antisymmetric stretching
ν_3(F_2)	370	__	MoO_4 : O-Mo-O bending
ν_3(F_2)	340	__	MoO_4 : O-Mo-O bending
Bg	188		
Eg	125-151	__	external Modes MoO_4^{2-}, and Zn^{2+} motions
Eg	78		

Conclusions

In this work, we prepared $ZnMoO_4$with a facile coprecipitation method. Structrual studies confirm the triclinic zinc molybdate according to the standard file referenced in the JCPDS database. The Thermal analyses show the decomposition behavior under air, a phase transition was observed at 466°C (Triclinic to monoclinic phase). All the Vibrational modes were detected and assigned, infrared and Raman bands have the same frequencies showing that the compound is non-centrosymmetric.

References

1. Zhuravlev V.D., Reznitskikh O.G., Velikodnyi Y.A., Patrusheva T.A., Sivtsova O.V., *J. Solid State Chem.* 184 (2011) 2785.
2. Ungelenk J., Speldrich M., Dronskowski R., Feldmann C., *J. Solid State Sci* .31 (2014) 62.
3. Tomaszewicz E., Kaczmarek S.M., Fuks H., *Mater. Chem. Phys.* 122 (2010) 595.
4. Tomaszewicz E., Kaczmarek S.M., Fuks H., *J. Rare Earth* 27 (2009) 569.
5. Lee G.H., Kang S., *J. Lumin.* 131 (2011) 2606.
6. Ait Ahsaine H., Taoufyq A., Patout L., Ezahri M., Benlhachemi A., Bakiz B., Villain S., Guinneton F., Gavarri J.-R., *J. Solid State Chem.* 218 (2014) 124.
7. Cavalcante L.S., Sczancoski J.C., Siu L.M., Longo E., Varela J.A., *Colloids Surf. A.* 396 (2012) 346.
8. Spassky D., Vasil'ev A., Kamenskikh I., Kolobanov V., Mikhailin V., Savon A., *Phys. Status Solidi a.* 206 (2009) 1579.
9. Nikolaenko T.N., Hizhnyi Y.A., Nedilko S.G., *J. Lumin.* 128 (2008) 807.
10. Ivleva L.I., Voronina I.S., Berezovskaya L.Y., Lykov P.A., Osiko V.V., Iskhakova L.D., *Crystallogr. Rep.* 53 (2008) 1087.
11. Mikhailik V.B., Kraus H., Wahl D., Ehrenberg H., Mykhaylyk M.S., *Nucl. Instr. Meth. Phys. Res.* 562 (2006) 513.
12. Arnaboldi C., Brofferio C., Cremonesi O., Gironi L., Pavan M., Pessina G., Pirro S.,Previtali E., *Astropart. Phys.* 34 (2011) 797.
13. Gironi L., Arnaboldi C., Beeman J.W., Cremonesi O., Danevich F.A.,Degoda V.Y., Ivleva L.I., Nagornaya L.L., Pavan M., Pessina G.,Pirro S.,Tretyak V.I.,Tupitsyna J., *J. Instrum.* 5 (2010) 11007.
14. Nagornaya L.L., Danevich F.A., Dubovik A.M., Grinyov B.V., Henry S., Kapustyanyk V., Kraus H., Poda D.V., Kudovbenko V.M., Mikhailik V.B., Panasyuk M., Polischuk O.G., Rudyk V., Tsybulskyi V., Tupitsyna I.A., Vostretsov Y.Y., *IEEE T. Nucl. Sci.* 56 (2009) 2513.
15. Beeman J.W., Bellini F., Capelli S., Cardani L., Casali N., Dafinei I., Di Domizio S., Ferroni F., Galashov E.N., Gironi L., Orio F., Pattavina L., Pessina G., Piperno G., Pirro S., Shlegel V.N., Vasilyev Ya V., Tomei C., Vignati M., *Astropart. Phys.* 35 (2012) 813.
16. Raj A.M.E.S., Mallika C., Swaminathan K., Sreedharan O.M., Nagaraja K.S., *Sens. Actuator B-Chem.* 81 (2002) 229.
17. Chen C.C., Jiang Y.R., Chang K.H., *Adv. Mat. Res.* 557 (2012) 761.
18. Lv L., Tong W., Zhang Y., Su Y., Wang X., *J. Nanosci. Nanotechnol.* 11 (2011) 9506.
19. Li Y., Weisheng G., Bo B., Kaijie G., *IEEE Int. Conf. Energ. Environ. Tech.* 3 (2009) 672.
20. Guo J., Zhou D., Wang H., Yao X., *J. Alloys Compd.* 509 (2011) 5863.
21. Leyzerovich N.N., Bramnik K.G., Buhrmester T., Ehrenberg H., Fuess H., *J. Power Sources* 127 (2004) 76.

22. Cavalcante L.S., Moraes E., Almeida M.A.P., Dalmaschio C.J., Batista N.C.,   Varela J.A., Longo E., Siu Li M., Andrés J., Beltrán A., *Polyhedron* 54 (2013) 13.
23. Lv L., Tong W., Zhang Y., Su Y., Wang X., *J. Nanosci. Nanotechnol.* 11 (2011) 9506.
24. Jiang Y.R., Lee W.W., Chen K.T., Wang M.C., Chang K.H., Chen C.C., *J. Taiwan Inst. Chem. Eng.* 45 (2014) 207.
25. Sotani N., Suzuki T., Nakamura K., Eda K., Hasegawa S., *J. Mat. Sci.* 36 (2001) 703.
26. Kruglyashov A.L., Skou E.M., *Solid State Ionics* 28 (1988) 233.
27. Manthiram A., Gopalakrishnan J., *Mat. Res. Bull.* 15 (1980) 207.
28. Dubovik AM., Vostretsov Y.Y., Grinyov B.V., Danevich F.A., Kraus H., Nagornaya L.L., Mikhailik V.B.,Tupitsyna I.A., *Acta Phys. Pol. A* 117 (2010) 15.
29. Bhuvana C.V., Viswanathan B., Sastri M.V.C., *Ind. J. Chem.* 1A (1979) 385.
30. Kurzawa M., Bosacka M., *J. Therm. Anal. Calorim.* 60 (2000) 177.
31. Ryu J.H., Koo S.M., Yoon J.W., Lim C.S., Shim K.B., *Mater.Lett.* 60 (2006) 1702.
32. Sen A.,Pramanik P., *Mater. Lett.* 50 (2001) 287.
33. Peng C., Gao L., Yang S., Sun J., *Chem. Comm.* 43 (2008) 5601.
34. Shahri Z., Bazarganipour M., Salavati-Niasari M., *Superlattices Microstruct.* 63 (2013) 258.
35. Ait ahsaine H., Taoufyq A., Ezahri M., Benlhachemi A., Bakiz B., Villain S., Arab M., Guinneton F., Gavarri J-R., *J. Mater. Environ. Sci.* 5 (2014) 2449.
36. Keereeta Y., Thongtem T., Thongtem S., *Mater. Lett.* 68 (2012) 265.
37. Liang Y., Liu P., Li H. B., Yang G. W., *Cryst. Growth Des.* 12 (2012) 4487.
38. Zhang G., Yu S., Yang Y., Jiang W., Zhang S., Huang B., *J. Cryst. Growth* 312 (2010) 1866.
39. Ait ahsaine H., Zbair M., Ezahri M., Benlhachemi A., Bakiz B., Arab M., Guinneton F., Gavarri J-R., *Ceram. Int.* 41 (2015) 15193.
40. Bhattacharya S.,Kar T., Bar T., Roy D.,Graca M.P.F., Valente M.A., *Sci. Adv. Mater.* 3 (2011) 284.
41. Keereeta Y.,Thongtem T., Thongtem S., *superlattices Microstruct.* 69 (2014) 253.
42. Subcik J., Koudelka L., Mosner P., Montagne L., Revel B., Gregora I., *J. Non-Cryst. Solids* 355 (2009) 970.
43. Bih L., Abbas L., Mohdachi S., Nadiri A., *J. Mol. Struct.* 891 (2008) 173.
44. ElBatal F.H., Abdelghany A.M., Elwan R.L., *J. Mol. Struct.* 1000 (2011) 103.
45. Basiev T.T., Sobol A.A., Voronko Y.K., Zverev P.G., *Opt. Mater.* 15 (2000) 205.
46. Aleksandrov L., Komatsu T., Iordanova R., Dimitriev Y., *Opt. Mater.* 33 (2011) 839.
47. Ait Ahsaine H., Ezahri M., Benlhachemi A., Bakiz B., Villain S., Valmalette J-C., Guinneton F., Arab M., Gavarri J-R., *RSC Advances.* 5 (2015) 96242.
48. Phuruangrat A., Thongtem T., Thongtem S., *J. Alloys Compd.* 481 (2009) 568.
49. Saraf U., Bajpal P.K., Chowdury R.N.P., *J. Int. Academ. Phys. Sci.* 14 (2010) 81.
50. Sejkora J., Čejka J., Malíková R., López A., Xi Y., Frost R. L., *Spectrochim. Acta A* 130 (2014) 83.

(2016) ; http://www.jmaterenvironsci.com/